Action potential-evoked Ca^{2+} signals and calcium channels in axons of developing rat cerebellar interneurones

Lia Forti, Christophe Pouzat and Isabel Llano

Arbeitsgruppe Zelluläre Neurobiologie, Max-Planck-Institut für biophysikalische Chemie, D-37077 Göttingen, Germany

(Received 11 February 2000; accepted after revision 17 May 2000)

1. Axonal [Ca^{2+}] transients evoked by action potential (AP) propagation were studied by monitoring the fluorescence of the high-affinity calcium-sensitive dye Oregon Green 488 BAPTA-1, introduced through whole-cell recording pipettes in the molecular layer of interneurones from cerebellar slices of young rats.

2. The spatiotemporal profile of Ca^{2+}-dependent fluorescence changes was analysed in well-focused axonal stretches a few tens of micrometres long. AP-evoked Ca^{2+} signals were heterogeneously distributed along axons, with the largest and fastest responses appearing in hot spots on average ~5 μm apart.

3. The spatial distribution of fluorescence responses was independent of the position of the focal plane, uncorrelated to basal dye fluorescence, and independent of dye concentration. Recordings using the low-affinity dye mag-fura-2 and a Cs^{+}-based intracellular solution revealed a similar pattern of hot spots in response to depolarisation, ruling out measurement artefacts or possible effects of inhomogeneous dye distribution in the generation of hot spots.

4. Fluorescence responses to a short train of APs in hot spots decreased by 41–76 % after bath perfusion of ω-conotoxin MVIIC (5–6 μM), and by 17–65 % after application of ω-agatoxin IVA (500 nM). ω-Conotoxin GVIA (1 μM) had a variable, small effect (0–31 % inhibition), and nimodipine (5 μM) had none. Somatically recorded voltage-gated currents during depolarising pulses were unaffected in all cases. These data indicate that P/Q-type Ca^{2+} channels, and to a lesser extent N-type channels, are responsible for a large fraction of the [Ca^{2+}] rise in axonal hot spots.

5. [Ca^{2+}] responses never failed during low-frequency ($\leqslant$ 0·5 Hz) stimulation, indicating reliable AP propagation to the imaged sites. Axonal branching points coincided with a hot spot in ~50 % of the cases.

6. The spacing of presynaptic varicosities, as determined by a morphological analysis of Neurobiotin-filled axons, was ~10 times larger than the one measured for hot spots. The latter is comparable to the spacing reported for varicosities in mature animals.

7. We discuss the nature of hot spots, considering as the most parsimonious explanation that they represent functional clusters of voltage-dependent Ca^{2+} channels, and possibly other [Ca^{2+}] sources, marking the position of developing presynaptic terminals before the formation of *en passant* varicosities.

Propagation of action potentials (APs) in neurones produces transient rises in cytosolic [Ca^{2+}] which, in axons, reach micromolar levels at highly localised presynaptic sites (Llinás *et al.* 1992), where they trigger neurotransmitter release. The spatial distribution and the origin of [Ca^{2+}] transients in axons remains, however, largely unexplored. A heterogeneous distribution of AP-evoked signals was found in crayfish axons (Delaney *et al.* 1991), lamprey motoneurones (Bacskai *et al.* 1995), lizard motor nerve terminals (David *et al.* 1997) and, in mammals, in rat hippocampal cultures (Mackenzie *et al.* 1996) and in the axon and calyx presynaptic terminal of neurones of the medial nucleus of the trapezoid body (MNTB; Borst *et al.* 1995). Axonal sites with large [Ca^{2+}] responses were either coincident with morphologically identified, large presynaptic terminals (Borst *et al.* 1995; David *et al.* 1997), or shown to coincide with *en passant* boutons (Mackenzie *et al.* 1996; Frenguelli & Malinow, 1996). Various hypotheses were made on the nature of the observed extrasynaptic AP-evoked signals, from pure diffusion from adjacent terminals (David

et al. 1997), to influx from low density pre-terminal (Borst *et al.* 1995) or intervaricosity (Mackenzie *et al.* 1996) Ca^{2+} channels. Homogeneous [Ca^{2+}] rises at axonal sites remote from presynaptic terminals in response to electrical stimulation have been observed, in mammals, in the unmyelinated proximal axon of rat neocortical pyramidal neurones (Schiller *et al.* 1995), of cerebellar Purkinje cells (Callewaert *et al.* 1996), and of cultured dorsal root ganglion cells (Lüscher *et al.* 1996), in axons of the adult and neonatal rat optic nerve (Sun & Chiu, 1999, and references therein) and unmyelinated nerve fibres of rat vagus nerve (Wächtler *et al.* 1998).

Voltage-dependent Ca^{2+} channel (VDCCs) types responsible for the presynaptic Ca^{2+} influx associated with evoked transmitter release have been identified in many preparations (reviewed by Dunlap *et al.* 1995; Iwasaki *et al.* 2000). In the mammalian central nervous system (CNS), immunocytochemical studies have revealed the presence of α_{1A} and α_{1B} Ca^{2+} channel subunits localised to presumed presynaptic terminals (Westenbroek *et al.* 1992, 1995), and α_{1A}, α_{1B} and α_{1E} subunits in the calyx terminal of the MNTB from young rats (Wu *et al.* 1999), while α_{1E} immunoreactivity was demonstrated in axons of Purkinje cells from the human cerebellum (Volsen *et al.* 1995). An involvement of axonal VDCCs in the generation of AP propagation failures (Lüscher *et al.* 1996) and in the regulation of firing rate through activation of Ca^{2+}-dependent K^+ channels (Callewaert *et al.* 1996) was proposed. In addition to activation of VDCCs, other mechanisms could, in principle, contribute to generate the axonal AP-evoked [Ca^{2+}] rises. Intracellular Ca^{2+} storage organelles have been observed in axons, and it has been debated whether release of Ca^{2+} from these organelles takes place at synapses or other axonal locations during spike conduction and synaptic transmission (reviewed by Ogden, 1996).

In the CNS of higher vertebrates, measuring AP-evoked fluorescence [Ca^{2+}] signals in axons is a difficult task because of their small size. Photodynamic damage caused by the intense illumination needed to resolve these signals is a major concern. A study from this laboratory has shown that in Cs^+-loaded cerebellar basket cells, depolarisation-evoked [Ca^{2+}] rises are heterogeneously distributed along the axon (Llano *et al.* 1997). In order to clarify the distribution and nature of Ca^{2+} sources under more physiological conditions, and to distinguish synaptic and extrasynaptic axonal sites, we now study the [Ca^{2+}] signals in the unmyelinated axons of basket and stellate cells of young rat cerebella during AP stimulation, using fluorescence [Ca^{2+}] imaging coupled to patch-clamp recordings. We describe the spatial patterns of the evoked [Ca^{2+}] transients and we study the sensitivity of [Ca^{2+}] signals to various VDCC blockers. By comparing the spatiotemporal [Ca^{2+}] dynamics with the distribution of varicosities in young and mature axons, as obtained by light microscopic examination of Neurobiotin-filled cells, we discuss the relation of [Ca^{2+}] 'hot spots' with presynaptic *en passant* terminals. In addition, we report on the [Ca^{2+}] signals observed at axonal branching points and their amplitude relative to the average hot spot signals.

METHODS

Preparation

Sagittal or parasagittal cerebellar slices (180 μm thick) were cut from the vermis of 12- to 16-day-old (P12–P16) Wistar rats, decapitated after either cervical dislocation or deep anaesthesia with Metofane (Janssen; 0·5 ml in 2 l administered for 1–2 min). Slices were incubated for at least 1 h at 32 °C in oxygenated bicarbonate-buffered saline (BBS) containing (mM): 125 NaCl, 2·5 KCl, 2 $CaCl_2$, 1 $MgCl_2$, 1·25 NaH_2PO_4, 26 $NaHCO_3$, 10 glucose, pH 7·4 when equilibrated with 95%O_2–5%CO_2. Slices were later transferred to the recording chamber and perfused with BBS (1–1·5 ml min^{-1}) at room temperature (20–23 °C). For fluorescence Ca^{2+}-imaging experiments, whole-cell recording (WCR) pipettes were filled with (mM): 150 KCl, 4·6 $MgCl_2$, 10 Hepes-K^+, 4 Na-ATP, 0·4 Na-GTP, and either 0·2 Oregon Green 488 BAPTA-1 (OG1; K_d for Ca^{2+} binding: 115 nM, according to our *in vitro* calibration, see below), 0·4 Calcium Green-5 (CG5; K_d: ~20 μM, Llano *et al.* 1997), or 0·4 mag-fura-2 (K_d: 25 μM, as reported by Molecular Probes), pH 7·3. In a few experiments KCl was replaced by potassium gluconate. In experiments using mag-fura-2, KCl was replaced with CsCl in the intracellular solution. In a separate series of whole-cell recordings used for morphological reconstruction of the axon, the pipette-filling solution also contained 1 mM EGTA, 0·2% Neurobiotin or 0·2% biocytin, and no fluorescent indicators. All chemicals were purchased from Sigma, except for OG1, CG5 and mag-fura-2 (Molecular Probes, Eugene, Oregon, USA), Neurobiotin/biocytin (Vector Laboratories, Burlingame, CA, USA), and Ca^{2+} channel blockers (see below).

Electrophysiology

Interneurones in the molecular layer were identified using an upright microscope (Axioscop, Zeiss, Germany) with Nomarski differential interference contrast (DIC) optics, a ×63, 0·9 NA water immersion objective, and a 0·63 NA condenser. Tight-seal WCRs were obtained with borosilicate pipettes (4–6 MΩ) from superficial somata using an EPC-9 amplifier (HEKA Electronik, Darmstadt, Germany). Series resistances ranged from 10 to 40 MΩ (50–70% compensated). To obtain a better control of spontaneous firing, axonal action potentials were evoked while keeping the soma in the voltage-clamp mode, by application of 0·5–3 ms long depolarising steps to 0 mV from a holding potential of −60 mV (Fig. 2*D*). This protocol produces unclamped spikes which propagate along the axon, as shown by Tan & Llano (1999).

Fluorometric calcium imaging

Digital fluorescence images were obtained using an excitation-acquisition system from T.I.L.L. Photonics (Planegg, Germany). Briefly, to excite fluorescence of the Ca^{2+} dyes OG1 and CG5, light from a 75 W Xe lamp was focused on a scanning monochromator set at 488 nm and coupled, by a quartz fibre and a lens, to the microscope, equipped with a dichroic mirror and a high-pass emission filter centred at 505 and 507 nm, respectively. In experiments using mag-fura-2, the monochromator was set at 390 nm; the dichroic mirror and the high-pass emission filter had centre wavelengths at 405 and 470 nm, respectively. Images were acquired by a Peltier-cooled PCO SensiCam camera (640 × 480 pixels; 0·25 μm pixel size after ×63 magnification) connected to a 12 bit A/D converter. After allowing > 7 min for dye loading in the axon, each experiment began with the search for a suitable axonal area. During this period, care was taken to minimise

exposure of the preparation to 488 nm light in order to limit photodamage (see below). The axon geometry was inferred from careful inspection of a few images (taken with 20–30 ms exposure time) at different z planes. During recordings, images were acquired with a 50 ms exposure/image, plus 2 ms between exposures, resulting in a 52 ms interval between images. In a few experiments, 70 ms exposures were used. The first 4 or 6 images were taken while holding the cell at −60 mV, and stimulation with a single depolarising pulse (0·5–3 ms long), or with a train of 2–8 such pulses (20 ms interval between pulses), was applied 2 ms after the start of the 5th or 7th image. The number of images acquired after stimulation varied between 4 and 22, corresponding to 208 to 1144 ms, so that a variable portion of the decay of fluorescence responses was recorded. The shortest acquisitions were used with the purpose of limiting phototoxic damage, mostly in experiments using repeated single pulse stimulation.

With repeated fluorescence acquisition sequences, phototoxic damage eventually developed, as identified by the following signs. (i) A large negative increase of the baseline inward current at −60 mV holding potential, from the accepted values of 0 to −70 pA, down to hundreds of pA; this was sometimes preceded by development of outward currents. (ii) A large increase in the electrical baseline noise. (iii) The appearance of long, squared inward currents (−200 to −550 pA) on the repolarisation phase after the stimulus pulse, with progressively longer duration (1–15 ms). (iv) The sudden inability of fluorescence levels to recover to baseline after stimulation, and failure of a subsequent AP to elicit a fluorescence transient. On average, a cumulative illumination of $13 \pm 4{\cdot}5$ s (range: 6·5–21·2 s) could be applied before development of these signs ($n = 15$ experiments). The illumination power, measured at the objective back-focal plane, varied from 1·5 to 2·4 mW (at 488 nm) during the time of the present study. Before development of the above phototoxic effects, acquisition of fluorescence images was paralleled by progressive run-down (Fig. 2*D*) of the peak inward (Na^+ current, as determined by TTX application; not shown) and outward currents recorded at the soma during the voltage step. Na^+ current run-down was more pronounced than in control, non-imaging WCRs (over ∼30 min: 32 ± 18% in control recordings, $n = 4$; 62 ± 18% in imaging experiments, $n = 12$). However, decrease of the fast inward current to 10% of its initial value did not prevent the generation and propagation of regenerative action potentials in the axon, as shown by the reliable presence of non-zero fluorescence responses in distal axons late in the recordings, with similar time courses to earlier responses (Fig. 2*B*). In some recordings, the 'beading' induced in neurites by mechanical- or photo-induced cell injury (e.g. Kriegstein & Dichter, 1983) was observed both in dendrites and axons, generally from the start of the recording. Such experiments were not analysed. Apart from slowly developing photodamage symptoms, we never observed bleaching of OG1 or CG5 basal fluorescence during individual stimulations. However, attempts to image AP-stimulated Ca^{2+} rises with the ratiometric indicator fura-2 were discouraged by the bleaching occurring with 380/360 nm excitation during a single stimulus.

Image analysis

Stimulus-induced fluorescence changes were analysed off-line along identified stretches of axon. A dotted line was drawn by eye through neighbouring pixels along the axon in the first image of a sequence (or of an averaged sequence), thus defining a one-dimensional array of pixels (axon array). For each pixel in the array, a measurement of the relative change in fluorescence, $\Delta F/F_o$, where F_o is the mean resting value, was obtained as follows. (a) For each consecutive nth image in the sequence, the average fluorescence $f(n,i)$ was obtained in a square 'box' of 5×5 pixels (unless otherwise specified), corresponding to $1{\cdot}25 \times 1{\cdot}25\ \mu m^2$, and centred on the ith pixel. (b) Background fluorescence was evaluated by copying the axon-outlining dotted line to a background area close to the axon (Fig. 3*A*) in every image, and the average fluorescence $B(n,i)$ was measured over a 9×9 pixel box around pixel i in the corresponding 'background array'. $B(n,i)$ was then subtracted from $f(n,i)$ for every n and i. (c) The background-subtracted fluorescence $F(n,i) = f(n,i) - B(n,i)$ was converted to:

$$\Delta F/F_o(n,i) = 100(F(n,i) - F_o(i))/F_o(i),$$

where $F_o(i)$ is the average resting fluorescence and $F_o(i) = \langle f(n,i) - B(n,i) \rangle_{rest}$. This background subtraction procedure was used to account for the inhomogeneities in background fluorescence, which can arise from outflow of dye from the pipette prior to seal formation. Maximum spatial fluorescence variations along 'background arrays' ranged from 0·5 to 10% of mean background counts ($2{\cdot}8 \pm 3$%, mean ± S.D., $n = 32$ cells). We excluded from analysis experiments where $B(n,i)$ had a time evolution correlated to the stimulus. When re-analysing the data with the background subtraction method described in Llano *et al.* (1997), positioning of hot spots (see below) was unchanged. The mean background counts in experiments using OG1 (200 μM) were $28{\cdot}4 \pm 12{\cdot}5$ (mean ± S.D., $n = 20$ cells, measured after subtraction of mean dark counts of our camera). Mean resting counts were $39 \pm 15{\cdot}3$ (mean ± S.D.). The ratio of resting to background counts across all axonal positions ranged from 1·09 to 3·35 (average ratio was $1{\cdot}48 \pm 0{\cdot}28$, mean ± S.D.). Interexperiment variability of the average background and axonal resting counts originates in part from changes in the illumination power over days. Analysis of images was performed with home-made routines within the IGOR programming environment (Wavemetrics, Lake Oswego, OR, USA).

We performed an *in vitro* calibration of OG1 fluorescence *vs.* $[Ca^{2+}]$ (as described in Tan & Llano, 1999, but using the experimental set-up described above and test solutions with $[Ca^{2+}]$ valves ranging from 17 nM to 1·35 μM). According to this calibration, and assuming a basal $[Ca^{2+}]$ of 40 nM, OG1 saturation should be reached for $\Delta F/F_o$ values of ∼380%. Thus the typical peak $\Delta F/F_o$ signal of ∼49% produced by a single AP stimulus (see Results) should correspond to $[Ca^{2+}]$ levels in the linear portion of the $\Delta F/F_o$–$[Ca^{2+}]$ relationship, far below saturating $[Ca^{2+}]$ levels. This allows estimation of the variability of $[Ca^{2+}]$ transients ($CV_{\Delta[Ca^{2+}]}$) from the variability of $\Delta F/F_o$. The coefficient of variation (CV) of peak $\Delta F/F_o$ signals was obtained (for 1 AP stimuli) as:

$$CV = \sqrt{\frac{(\sigma^2_{peak} - \sigma^2_{rest})}{\langle \text{peak } \Delta F/F_o \rangle}},$$

where σ^2_{peak} and σ^2_{rest} are variances calculated from successive responses for peak $\Delta F/F_o$ and for $\Delta F/F_o$ at the time point before stimulation, respectively. CV is independent of baseline variability and thus estimates $CV_{\Delta[Ca^{2+}]}$. It is, however, likely to be an overestimate, because σ^2_{peak} includes noise arising from detection of increased light levels during the AP-evoked Ca^{2+} rise, as OG1 increases its fluorescence upon binding Ca^{2+} (see discussion in Mackenzie *et al.* 1996). A further factor producing overestimation of $CV_{\Delta[Ca^{2+}]}$ is the slow run-down of mean $\Delta F/F_o$ described in Fig. 2*E*.

Detection of hot spots

We define a calcium hot spot as an axonal position where $\Delta F/F_o^{stim}$, defined as the $\Delta F/F_o$ value in the 50 ms window after stimulus onset, had a local maximum in space (i.e. a maximum in the plot of $\Delta F/F_o^{stim}$ *vs.* i; where i is a pixel in the axon array). As noise in the $\Delta F/F_o$ measurement could induce the appearance of artefactual maxima, or produce uncertainty in their positioning, criteria were

sought to exclude such cases. We accepted a local maximum as a hot spot in cases where, in the axonal region between the maximum position ± 1·5 μm, a maximum was present for every possible curve $f(i)$ with values in the surface delimited by: $\Delta F/F_o^{stim}(i) + \sigma(i)$ and $\Delta F/F_o^{stim}(i) - \sigma(i)$ ('confidence' surface; $\sigma(i)$ is the standard deviation of $\Delta F/F_o$ values computed for site i during the pre-stimulus recording time; see Fig. 1). Detection of hot spots was done by visual examination of the confidence surface, after smoothing $\Delta F/F_o^{stim}$ and $\Delta F/F_o^{stim} \pm \sigma$ with a 3 points moving average. Figure 1 illustrates detection criteria applied in two different axons. On the left, $\Delta F/F_o^{stim}$ is plotted *vs.* i and identified hot spots are marked with filled triangles. In some regions (enlarged examples in Fig. 1, insets), noise around local maxima was too large to confirm the presence of a Ca^{2+} source or to allow its positioning. Inflections in the $\Delta F/F_o^{stim}$ *vs.* i plot were often present on one or both sides of hot spots (arrows). This might indicate that some local maxima in the plot could have gone undetected due to our limited space resolution. The presence of hot spots was studied both in experiments using single APs (Fig. 1*A*) or trains of APs (Fig. 1*B*). In both cases, hot spots were detected by analysing $\Delta F/F_o$ values in the 50 ms time window after stimulation onset, which reflects the $[Ca^{2+}]$ rise due to 1–2 APs (interpulse interval was 20 ms). In cells where different types of stimuli were applied, the position of hot spots was independent of stimulus type.

For measurement of hot spot peak amplitudes, the spots included were detected with the more restrictive confidence surfaces constructed using $2\sigma(i)$ instead of $\sigma(i)$. Measurement of 'cold spot' properties (see Results) was obtained from sites corresponding to a minimum of the $\Delta F/F_o^{stim}$ *vs.* i plot, and located between a couple of adjacent hot spots for which a distance could be measured. Results from pooled data are given as means ± S.D. Statistical comparisons were made with the Mann-Whitney U test unless specified.

Ca^{2+} channel pharmacology

For this series of experiments P13–P15 rats were used. Ca^{2+} channel blockers were dissolved in BBS and bath applied during imaging experiments. When using bath application of Cd^{2+}, NaH_2PO_4 was omitted in the extracellular BBS and NaCl was raised to 126·5 mM. Stock solutions of ω-conotoxin MVIIC (ω-CgTX-MVIIC; Tocris, UK), dissolved in BBS at 50 μM, ω-agatoxin IVA (ω-Aga-IVA; Peptide Institute, Japan) and ω-conotoxin GVIA (Alomone Labs, Israel), dissolved in H_2O at 50 and 100 μM, respectively, were frozen in liquid N_2, stored at −80 °C and used within 2 weeks. To prevent non-specific binding of peptide toxins, cytochrome c was added to stock solutions (at 1 mg ml^{-1}) and to BBS (at 0·1 mg ml^{-1}), both during the control period and throughout the drug perfusion. Nimodipine (Calbiochem) was

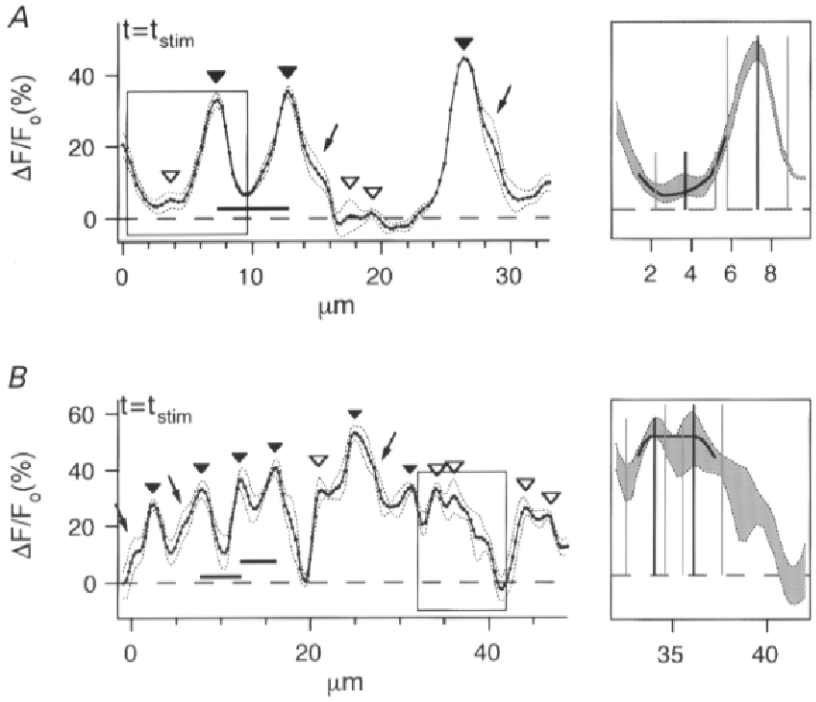

Figure 1. Detection of calcium hot spots and measurement of inter-hot spot distance

A and *B*, plot of $\Delta F/F_o^{stim}$ *vs.* position in the axon (continuous lines with symbols), for two different interneurones, illustrating application of criteria for detection of hot spots and for measurement of their distances (see text). Dotted lines plot $\Delta F/F_o^{stim} + \sigma$ and $\Delta F/F_o^{stim} - \sigma$ *vs.* axonal position i (in μm). Maxima identified as hot spots are marked ▼; noisy maxima, ▽; arrows on the inflections at the side of some hot spots indicate sites for possible undetected additional Ca^{2+} sources; thick horizontal bars connect couples of hot spots for which a distance was measured. *A*, axon stimulated with 1 AP. *B*, axon of a stellate cell stimulated with 8 APs. *A* and *B* insets: the plots expand the regions enclosed in boxes in *A* and *B*, respectively, to illustrate the criteria for rejection of noisy (leftmost maximum in *A*, inset) or badly positioned maxima (leftmost maximum in *B*, inset). $\Delta F/F_o^{stim}(i)$ is not plotted. Dotted lines indicate $\Delta F/F_o^{stim} \pm \sigma(i)$, and the enclosed confidence surface is coloured grey. Vertical lines indicate the position of local maxima for $\Delta F/F_o^{stim}(i)$ (thick lines) and of maxima ± 1·5 μm (thin lines). The thick curves are representative functions that have no maximum within ± 1·5 μm from the thick vertical lines.

dissolved in DMSO at 60 mM and stored at −20 °C. The efficacy of this stock was ascertained from block of L-type channel-mediated Ba^{2+} currents evoked by pulsing from −60 to −10 mV in whole-cell clamped mouse cerebellar granule cells at 5 days in culture. The ionotropic glutamate receptor blockers 2,3-dihydroxy-6-nitro-7-sulphamoyl-benzene(*f*)quinoxaline (NBQX; 10 μM) and D-amino-phosphonovalerate (APV; 50 μM) were also added to control- and drug-containing BBS. Imaging experiments aimed at studying Ca^{2+} channel pharmacology were performed both with the standard imaging set-up described above, and with the 2-photon laser excitation scanning set-up described by Tan & Llano (1999). In the latter case, due to the highly restricted localisation of fluorescence excitation, photodamage was significantly reduced, and run-down of somatic voltage-gated currents during depolarising pulses was absent (Tan & Llano, 1999). In this series of experiments, run-down of the axonal peak $\Delta F/F_o$ signals was similar in the two set-ups, and results of pharmacological experiments were compatible, so that they were pooled together. Data from cells with initial run-down larger than 60 % $(10\ min)^{-1}$ were discarded.

When studying the behaviour of peak $\Delta F/F_o$ in four control experiments using the same illumination frequency and intensity as in the drug test experiments, in two cases we noticed a fast run-down occurring in the first few minutes of image acquisition (19 and 23 % in 5 and 3 min, respectively; percentage run-down was estimated from linear fit to the peak $\Delta F/F_o$ values in the time window of interest), followed by a much slower decrease (10 and 4 % in 30 min) (Fig. 6*A*). A similar decrease in speed of run-down was noticed in the control period of a few drug test experiments (2 out of 22). On the contrary, we never observed spontaneous increases in the speed of run-down in the course of control experiments. Similarly, fast bath application of physiological saline had no effects on its own. On average, over the entire course of 20–40 min acquisition, $\Delta F/F_o$ responses declined by 11 ± 8 % $(20\ min)^{-1}$ (or $3{\cdot}8 \pm 1{\cdot}4$ % $(5\ s)^{-1}$ of cumulative illumination; 4 cells). Overall, these data show that the procedure adopted to estimate the percentage signal inhibition by applied blockers (see Results) might possibly underestimate, but should not overestimate, such inhibition.

Morphology

Intervaricosity spacing and axonal lengths were measured from Neurobiotin-filled neurones in embedded diaminobenzidine- and nickel-stained slices according to the procedure described in Pouzat & Hestrin (1997). Cells were drawn with a drawing tube attached to the microscope, and the length of the axonal arborisation for each interneurone was estimated from the drawing. This procedure provides an underestimate of the true length, because no correction was applied for the compression of the three-dimensional axonal structure onto the two-dimensional plane of the drawing.

RESULTS

General properties of axonal AP-evoked $[Ca^{2+}]$ signals

Stellate and basket cells in the molecular layer of thin parasagittal cerebellar slices from P12–P16 rats were loaded through patch-clamp pipettes with a K^+-based intracellular solution containing the Ca^{2+}-sensitive fluorescent indicator Oregon Green BAPTA-1 (OG1; 200 μM). The cell axon was identified in fluorescence images as a process originating from the soma or from a dendrite, and extending for a few hundreds of micrometres, well beyond the dendritic arborisation (Ramón y Cajal, 1911).

Figure 2*A* displays the pseudo-colour images recorded from a short segment of a stellate cell axon at rest and after a single AP. The plots in Fig. 2*B* show the fluorescence signals elicited in two selected axonal regions of $0{\cdot}56\ \mu m^2$ area (3×3 pixels) analysed in terms of the change in fluorescence normalised to the pre-stimulus levels ($\Delta F/F_o$, see Methods). The superimposed traces show that repeated stimulation with single APs reproducibly evoked detectable $[Ca^{2+}]$-dependent fluorescence changes at both axonal spots. Only the initial time course of responses is imaged in this experiment, to limit phototoxic effects of illumination (see Methods; see Figs 4 and 8 for examples of responses on a longer time scale). Fluorescence recovered to basal levels in between individual stimuli. No failures in the $[Ca^{2+}]$ signal in response to low frequency ($\leqslant 0{\cdot}5$ Hz) 1 AP stimulation were ever observed, either in the main axonal branch (71 stimuli in 12 cells, distances from the soma: 80 to 150–200 μm), or in the second and third order collateral branches (43 stimuli in 2 cells, at >100 μm from the cell soma). The same result was obtained from cells loaded with the low affinity Ca^{2+}-indicator Calcium Green-5N (CG5, 400 μM; not shown), where responses to single AP stimulation were recorded in the main axon branch and in first order collaterals (48 stimuli in 5 cells). The faithful appearance of $[Ca^{2+}]$ responses shows that no failures of AP propagation to the imaged axon branches ever occurred in our recording conditions. Variability of peak $\Delta F/F_o$ was analysed for the axonal spot with the best signal-to-noise ratio (spot *a* in Fig. 2*A*). An upper limit to the coefficient of variation (CV; see Methods) in this spot was estimated from 20 individual responses as 0·2, and in two other spots from two different cells as 0·17 (from 18 responses) and 0·24 (from 17 responses). Given the linear dependence of $\Delta F/F_o$ on $\Delta[Ca^{2+}]$ in the range of signals considered here, these values can be assumed to reflect $\Delta[Ca^{2+}]$ variability. They are in agreement with a previous report from presynaptic boutons in hippocampal cultures (Mackenzie *et al.* 1996).

The two spots analysed in Fig. 2*B* differed considerably in terms of signal amplitude and kinetics (compare the averaged $\Delta F/F_o$ time courses in Fig. 2*C*). These results suggest a spatial heterogeneity of $[Ca^{2+}]$ changes along axons, as previously observed for the depolarisation-evoked axonal $[Ca^{2+}]$ transients in Cs^+-loaded basket cells imaged with CG5 (Llano *et al.* 1997).

The stability of the fluorescence signals from the axonal area shown in Fig. 2*A* was studied by monitoring the response to single APs over a period of ∼10 min. Figure 2*E* plots the peak of the $\Delta F/F_o$ responses to such stimuli as a function of WCR time for spot *a*. A linear regression analysis shows that mean peak amplitude decayed by 23·4 % over 20 stimulation–acquisition cycles (cumulative illumination time: 12 s). On average, the mean peak $\Delta F/F_o$ declined by $6 \pm 2{\cdot}8$ % for 5 s of cumulative illumination (corresponding to 8–13 stimuli given in time windows of 25 s to 6–7 min; $n = 4$ cells). The small peak variability and the stability of

$\Delta F/F_o$ signals obtained with low frequency AP stimulation over time windows of a few minutes justifies the procedure of signal averaging for improvement of the signal-to-noise ratio in some of the analysis presented below.

Spatial heterogeneity of $[Ca^{2+}]$ responses: 'hot spots'

In order to characterise the spatiotemporal properties of AP-evoked axonal $[Ca^{2+}]$ transients, we analysed the $[Ca^{2+}]$ dynamics along continuous axon stretches (10–60 μm long) in 23 cells. Stimuli were applied consisting of single APs or of trains of 2, 4 or 8 APs with pulse intervals of 20 ms. Due to our time resolution, $\Delta F/F_o$ time courses showed a single peak for all types of stimuli. For each cell, an averaged sequence of fluorescence images was formed from 1 to 20 consecutive identical stimuli applied during time windows of <4 min. A dashed line was drawn through individual pixels in the axon, as exemplified in Fig. 3*A*, and the $\Delta F/F_o$ signals were calculated for each image as a function of position (i) along the line (see Methods). The resulting three-dimensional plot of $\Delta F/F_o$ *vs.* i and time is shown for one of these experiments in Fig. 3*B*. Inspection of this plot and of the initial $\Delta F/F_o$ time course at chosen positions (Fig. 3*C*) confirms that responses are heterogeneous all along the axon, with alternate large and small peak amplitudes and variable rise times. We defined as 'hot spots' the sites where the post-stimulus response ($\Delta F/F_o^{stim}$) had a local maximum in space. The criteria adopted to exclude noise artefacts when detecting hot spots are detailed in Methods (see also Fig. 1). In interneurones subjected to 1 AP stimulation, the average hot spot peak $\Delta F/F_o$ was 49 ± 21 % (50 ms exposure per image, $n = 29$ spots, 10 cells). Rise was generally complete within 52 ms (i.e. the acquisition time for one image). In hot spots stimulated with 2, 4 or 8 APs (43 Hz), peak $\Delta F/F_o$ values were 62 ± 17 % (2 APs; $n = 16$, 5 cells), 134 ± 36 % (4 APs; $n = 17$, 5 cells), and 157 ± 39 % (8 APs; $n = 32$, 9 cells). Rise was complete within 52–104 ms (2 APs), 104–156 ms (4 APs) and 208 ms (8 APs).

We estimated the distance between hot spots by searching for couples of such consecutive spots and requiring that $\Delta F/F_o^{stim}$ between them had a single minimum and no inflections. In 48 couples of hot spots from 18 cells (18 couples in 1 AP-stimulated axons; 30 couples with >1 AP; see Fig. 1), the mean distance was $4{\cdot}7 \pm 1{\cdot}5$ μm (no significant differences between different types of stimulations, $P = 0{\cdot}5581$). Distances between hot spots in stellate cells (24 couples, 10 cells) and in basket cells (24 couples, 8 cells) did not differ significantly ($P = 0{\cdot}9589$) (see below for the criteria used to distinguish stellate and basket cells).

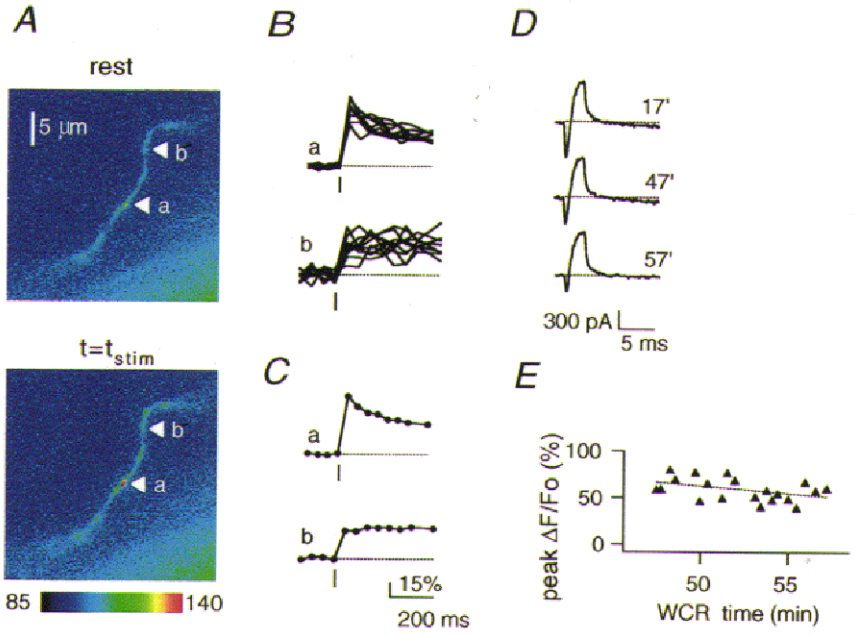

Figure 2. Fluorescence signals evoked in axons by a single action potential

A, fluorescence images of the axon of a P12 stellate cell (main branch ~100 μm from the cell body) filled with OG1 (200 μM) at rest (top) and in the 50 ms window after the onset of stimulation with a single AP (bottom). Calibration bar indicates arbitrary fluorescence units. *B*, superimposition of individual $\Delta F/F_o$ time courses from positions *a* and *b* of the axon in panel *A*, during 10 consecutive 1 AP stimulations in the time window 47–52 min after start of the whole-cell recording (WCR). Only the early phase (416 ms) of fluorescence responses was imaged in order to limit phototoxic damage. Note that the fluorescence response does not fail over 10 stimuli. *C*, the averages of responses presented in *B*. Notice the difference in kinetics and peak amplitude. *D*, whole-cell currents (leak subtracted) during the 3 ms depolarising stimuli applied at the indicated times in WCR. Note the progressive decrease of the inward voltage-dependent (Na^+ mediated) current (at 57 min it was 19 % of the value at 3 min). *E*, plot of peak $\Delta F/F_o$ *vs.* WCR time for spot *a* in panel *A*. Slope of linear fit (dotted line) is $-1{\cdot}55$ % min^{-1}.

In axonal positions where $\Delta F/F_o^{stim}$ had a minimum (cold spots), the peak response ranged from nearly zero up to substantial fractions of hot spot values (mean $\Delta F/F_o$: $29 \pm 9\%$, $n = 18$ spots, 7 cells; 1 AP stimulation) (examples in Figs 2*C*, 3*C* and 4*D*). In most of these cases, peak $\Delta F/F_o$ was reached more slowly than in hot spots, with a mean rise time of 162 ± 87 ms ($n = 18$ spots, 7 cells, 1 AP stimulation).

Hot spots are not a measurement artefact

To check whether the spatial heterogeneity of $\Delta F/F_o$ transients could be an artefact due to different distances of the imaged structures with respect to the focal plane, single AP-evoked responses were collected from the same axon at different focal planes (Fig. 4*A*). As expected from light scattering, defocusing of dye-filled structures by about ± 1 μm above and below the 'best' focal plane produced, in most axonal sites, a decrease in the average basal fluorescence F_o and a correlated noise increase (Fig. 4*B*). Nevertheless, $\Delta F/F_o^{stim}$ had only small variations, compatible with the previously mentioned time-dependent run-down. The heterogeneous spatial pattern of $\Delta F/F_o^{stim}$ was preserved across different focal planes (3 experiments; Fig. 4*C* and *D*). This demonstrates that spatial variability of the $[Ca^{2+}]$ signal is not merely a consequence of uneven focusing and of changes in the signal-to-noise ratio, but indicates the presence of areas sustaining different $[Ca^{2+}]$ transients. This could originate from various mechanisms. A possible artefactual origin for uneven $[Ca^{2+}]$ transients comes from an uneven cytosolic dye concentration along the axon, possibly because of binding to some immobile intracellular constituents. Differences in dye concentration could produce a variable exogenous buffer effect, blunting $[Ca^{2+}]$ transients to a variable extent along the axon. To check for this hypothesis, we studied the spatial distribution of fluorescence responses in axons filled with the low-affinity dye mag-fura-2 (400 μM). In order to elicit detectable signals, we used a Cs^+-based intracellular solution, and we applied 20–100 ms long depolarising pulses (to −10 or 0 mV) at the soma. In three experiments, we observed in axons a pattern of hot and cold spots compatible with the pattern described above for the case of 200 μM OG1, with a mean hot spot distance of

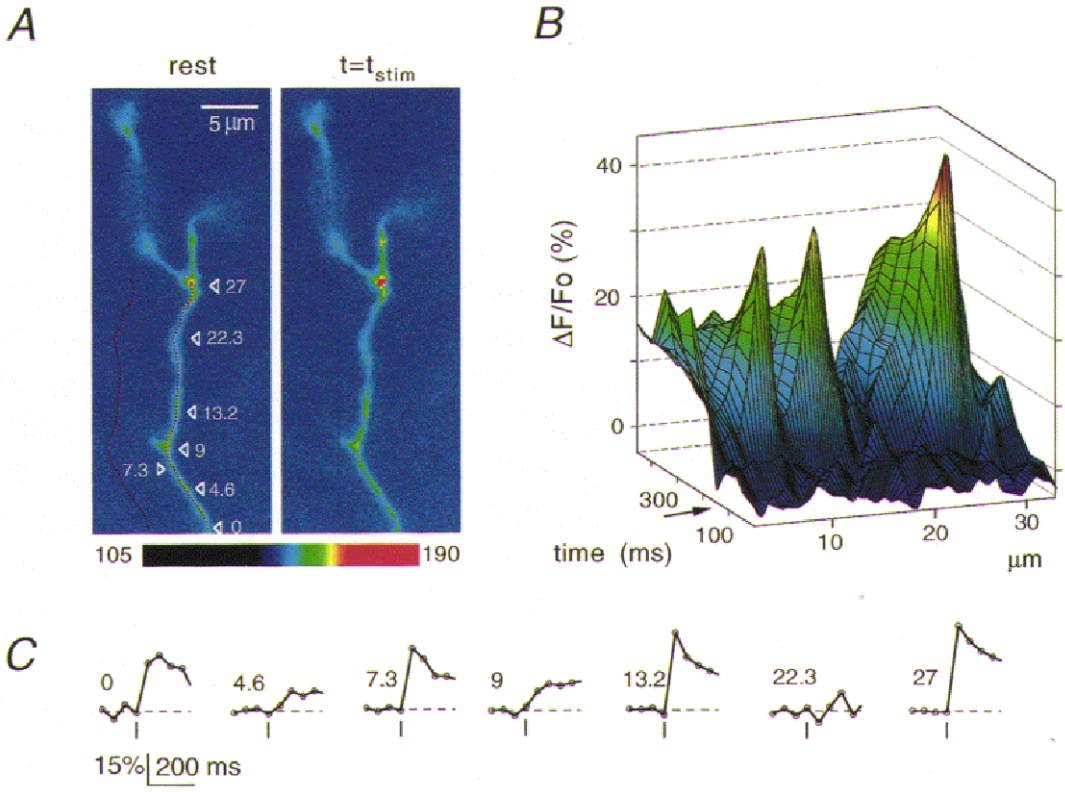

Figure 3. The spatial distribution of fluorescence calcium responses in axons

A, fluorescence images of the axon of a P13 stellate cell (2nd order collateral, ~100 μm from the cell body) filled with OG1 (200 μM) at rest (left) and after stimulation with a single AP (right). Images are averaged over 7 stimulation protocols. $\Delta F/F_o$ was measured for all pixels along the red dotted curve superimposed on the axon in the left image; the leftmost dotted curve was used for measurement of background as explained in Methods. Numbers in the image correspond to μm on the space axis of the plot in panel *B*. *B*, three-dimensional plot of $\Delta F/F_o$ *vs.* time (1 AP stimulus given at time indicated by the arrow) and *vs.* position along the axon for the same cell as in *A*. Note the consecutive peaks and valleys corresponding to axonal positions with large and fast, or small and slow responses to stimulation. *C*, initial time courses of $\Delta F/F_o$ for the seven axonal positions indicated in panel *A*. Traces show heterogeneity of signal peak amplitude and rise time. Bars below traces indicate stimulation time.

$4 \pm 1{\cdot}3$ μm ($n = 7$ spots) and with a clearly faster speed of rise (time to 50% peak) for $\Delta F/F_o$ in hot *vs.* cold spots ($P < 0{\cdot}005$, Wilcoxon matched-pairs test; Fig. 5). Moreover, in three experiments using a low OG1 concentration (50 μM), standard KCl-based solutions and 1 AP stimulation, hot and cold spots were observed with a mean hot spot distance of $4{\cdot}2 \pm 1{\cdot}1$ ($n = 8$). In particular, the rise time and peak amplitude in cold spots was not significantly different from the case of 200 μM OG1 (with 50 μM OG1, rise time: 168 ± 133 ms, $n = 8$ spots, $P > 0{\cdot}8$; peak $\Delta F/F_o$: 26 ± 19%, $n = 8$, $P > 0{\cdot}5$). In summary, the above observations rule out an artefactual origin for inhomogeneous fluorescence responses linked to the measurement condition or to effects secondary to the presence of dye.

Another possible mechanism for the production of variable $[Ca^{2+}]$ elevation is suggested by geometrical considerations. Changes in axonal diameter would produce a variable surface-to-volume ratio (S/V), and activation of homogeneously distributed membrane Ca^{2+} channels would yield a lower bulk $[Ca^{2+}]$ elevation in regions with smaller S/V. However the largest and fastest signals (the hot spot responses) arose both from large- and small-diameter sites, as defined by visual inspection of resting fluorescence images (compare peak $\Delta F/F_o$ in Fig. 3*C* for sites at $i = 7{\cdot}3$, $13{\cdot}2$ and 27 μm in Fig. 3*A*). Moreover, the majority of large-diameter sites contained a hot spot (31 of 41 visually identified 'large' sites from 20 cells). Thus, the observed spatial distribution of $[Ca^{2+}]$ rises in axons could be explained by mere surface/volume effects only after adding the accessory hypothesis that most of the volume in large-diameter sites is not accessible to the dye, e.g. because it is occupied by intracellular organelles. This is unlikely, since the accessible volume in a large CNS presynaptic terminal has been estimated to be close to the total terminal volume (Helmchen *et al.* 1997). A more plausible explanation for the spatial profile of the $[Ca^{2+}]$ signals is that of a heterogeneous

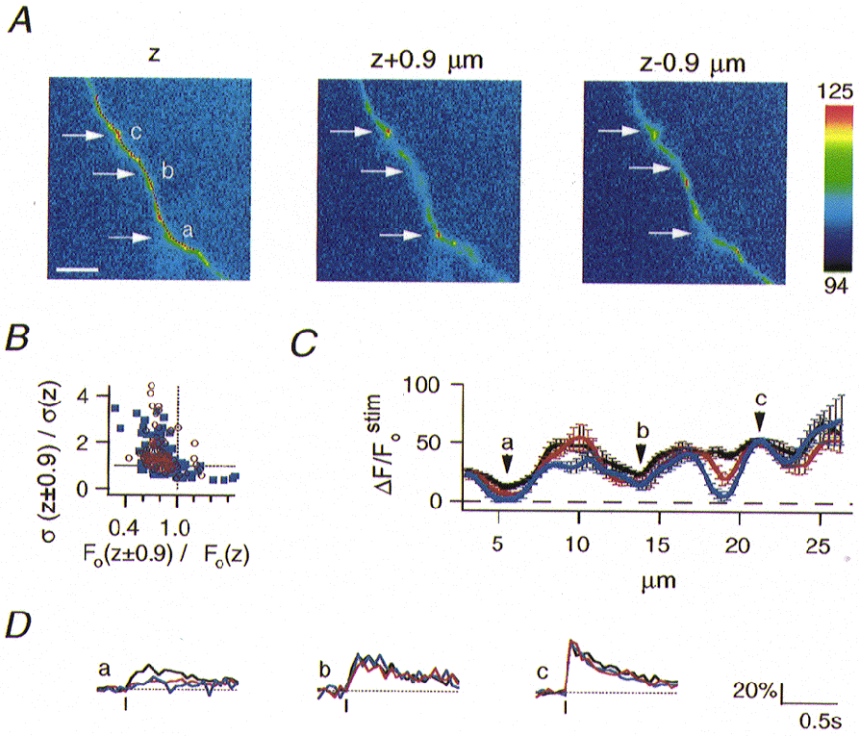

Figure 4. Effects of defocusing on axonal calcium signals

A, images of a 2nd order axon collateral (~80–110 μm from the soma of a P16 basket cell) taken at three different focal planes displaced by $\pm 0{\cdot}9$ μm (vertical displacement is marked above images) during the 50 ms window after the onset of stimulation with a single AP. Images are from averaged sequences (6 stimuli given at 20 s intervals for each focal plane; z plane imaged first, followed by $z + 0{\cdot}9$ μm plane and later $z - 0{\cdot}9$ μm plane). The dotted curve in the left image indicates the analysed axon region; an identical curve could be used to describe the axon in all focal planes, after offsetting by 2–4 pixels in the image plane. Scale bar: 5 μm. *B*, plot of the standard deviation (σ) of the resting $\Delta F/F_o$ *vs.* the corresponding basal fluorescence F_o in all analysed axonal positions at focal plane $z + 0{\cdot}9$ μm (red circles) and $z - 0{\cdot}9$ μm (blue squares). Both σ and F_o are normalised to the corresponding values in plane z. *C*, plot of $\Delta F/F_o^{stim}$ at focal planes z (black line), $z + 0{\cdot}9$ μm (red line), $z - 0{\cdot}9$ μm (blue line) *vs.* position in the axon. Error bars represent σ. The general decrease of $\Delta F/F_o$ with respect to z plane values (mean ratios are $0{\cdot}8$ and $0{\cdot}7$) can be explained by time-dependent run-down. Note that the spatial pattern of calcium responses does not change (apart from one exceptional site at ~19 μm, where the response was lost after defocusing). *D*, time course of $\Delta F/F_o$ at focal plane z (black traces), $z + 0{\cdot}9$ μm (red traces) and $z - 0{\cdot}9$ (blue traces) for positions *a*, *b* and *c* shown in panel *A*.

distribution of key molecules involved in Ca^{2+} signalling, including voltage-gated Ca^{2+} channels and/or intracellular Ca^{2+}-release channels, Ca^{2+} buffering and/or sequestration and extrusion systems.

Ca^{2+} channel types contributing to axonal Ca^{2+} rises

We investigated the nature of voltage-dependent Ca^{2+} channels involved in producing AP-stimulated axonal Ca^{2+} rises by combining imaging experiments and pharmacological manipulations using various Ca^{2+} channel blockers. To limit the photodamage associated with the repeated fluorescence excitation needed to acquire long sequences of control and test Ca^{2+} responses, 40 % of the monochromator light was cut with a neutral density filter. 4 AP stimuli, applied every 1–3 min, were used in order to obtain large, well-detectable responses. The time courses of peak $\Delta F/F_o$ at all identified hot spots of each axon were pooled together, and values during at least 10 min in control conditions and after drug application were compared (Fig. 6). In most experiments (13 out of 19), run-down of Ca^{2+} signals was visible in the initial control period (28 ± 15 % per 10 min, $n = 13$ cells, range 8–55 %; see Fig. 6*A* and *B*). To attempt a compensation of measurement errors introduced by run-down, inhibition was estimated as the percentage difference between the peak $\Delta F/F_o$ after several minutes of drug application and a decaying baseline extrapolated from a linear fit to the control period (Fig. 6*B*). As discussed in Methods, this procedure might possibly underestimate, but should not overestimate, the inhibitory effects of applied blockers.

In four out of four experiments ω-CgTX-MVIIC (5–6 μM), which potently blocks native N- and P/Q-type Ca^{2+} currents (Hillyard *et al.* 1992; Randall & Tsien, 1995; McDonough *et al.* 1996), as well as some toxin-resistant, R-type current components (Wu & Saggau, 1995; McDonough *et al.* 1996), decreased the AP-evoked Ca^{2+} rises. The inhibition can be seen as a clear change of slope in the plot of $\Delta F/F_o$ *vs.* time (Fig. 6*B*). After 8–12 min of continuous drug perfusion a maximal inhibition of 50 ± 17 % was reached (range: 41–76 %; Fig. 6*E*). This effect was clearly irreversible in three experiments where wash-out was obtained (example in Fig. 6*B*), arguing against a large contribution of N-type channels (Grantham *et al.* 1994; McDonough *et al.* 1996). These results show that activation of ω-CgTX-MVIIC-sensitive channels is necessary to generate a large fraction of AP-evoked Ca^{2+} rises in hot spots.

To further distinguish between channel types, we studied the effect of 500 nM ω-Aga-IVA, expected to block P- and Q-type Ca^{2+} currents (Mintz *et al.* 1992; Randall & Tsien, 1995). In all cells tested, ω-Aga-IVA inhibited the Ca^{2+} responses. The maximal effect (39 ± 17 %; range: 17–65 %, $n = 6$) was reached in 5–9 min (Fig. 6*C* and *E*) and was irreversible in the four cells in which wash-out was tested (example in Fig. 6*C*). P/Q-type channel activation thus controls the largest fraction of the ω-CgTX-MVIIC-sensitive hot spot Ca^{2+} responses.

The N-type channel blocker ω-conotoxin GVIA (1 μM) had no effect in one cell and only a small inhibitory effect in three more cells. The maximal block was reached in 3–10 min (mean inhibition: 17 ± 14 %, $n = 4$ cells, range: 0–31 %, Fig. 6*E*). Nimodipine (5 μM) had no effects in five cells tested (Fig. 6*E*). These data demonstrate a small contribution of N-type channels, but not of L-type channels, to the Ca^{2+} rises evoked by APs in axonal hot spots. Finally, axonal Ca^{2+} signals were strongly depressed (by 50–80 %) after 4–6 min bath application of 10 μM Cd^{2+}. Signals partially recovered upon Cd^{2+} wash-out ($n = 3$ experiments, 8 AP stimulation).

A fraction of the experiments described in this section was performed using a 2-photon laser excitation scanning set-up (see Methods). With this system, the voltage-dependent

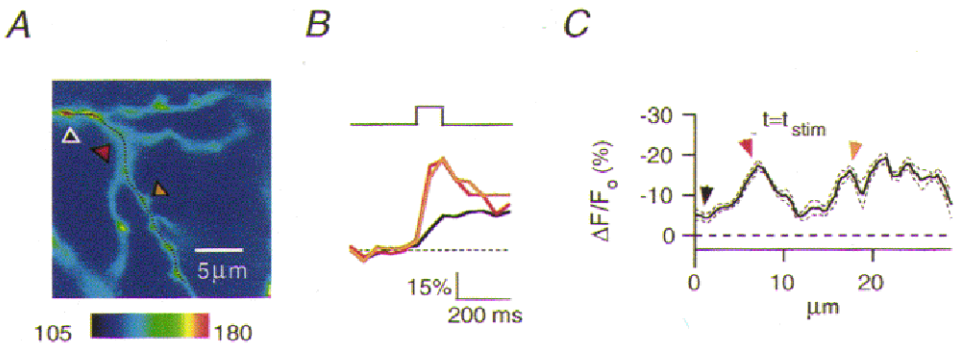

Figure 5. Depolarisation-evoked Ca^{2+} signals reported by the low-affinity dye mag-fura-2

Ca^{2+} signals evoked in the axon of a voltage-clamped basket cell in response to a 100 ms long pulse depolarisation from −60 to 0 mV. A Cs^+-based pipette solution containing 400 μM mag-fura-2 was employed. *A*, the imaged axon region at rest. The dotted curve superimposed on the axon indicates the analysed region. *B*, colour-coded $\Delta F/F_o$ responses for the axonal sites indicated by corresponding arrows in *A*. Stimulus protocol indicated above. Note the differences in rise time and peak values for the Ca^{2+} responses from the various axonal sites. *C*, plot of $\Delta F/F_o^{stim}$ *versus* axonal position. Colour-coded arrows correspond to traces in *B* and axonal sites in *A*. Note the presence of several hot spots, in analogy with results obtained using the high-affinity dye Oregon Green 488 BAPTA-1.

currents recorded at the soma during AP stimulation are remarkably stable over long (up to 2 h) recording times in control conditions (Tan & Llano, 1999). Application of the Ca^{2+} channel blockers ω-CgTX-MVIIC ($n = 1$), ω-Aga-IVA ($n = 3$), ω-conotoxin GVIA ($n = 3$) and nimodipine ($n = 3$) did not significantly modify inward Na^+ currents (Fig. 6*D*). Similarly, bath application of Cd^{2+} (50 μM) in whole-cell voltage-clamped interneurones did not alter the amplitude of the 1 ms pulse-evoked inward Na^+ current recorded at the soma ($n = 4$ cells), while blocking GABA release from the axon (Pouzat & Marty, 1999). The lack of effects of these blockers on somatic currents during AP stimulation suggests that the degree of activation of the blocker-sensitive Ca^{2+} channels located in the somatic and/or perisomatic region does not influence AP generation. Furthermore, we never observed a total failure of propagation of the AP train to any of the visualised axonal regions, as inferred from the clear presence of some degree of fluorescence responses after each stimulus. The spatial profiles of $\Delta F/F_o^{stim}$ were in all instances homogeneously affected by blockers (not shown), arguing against a differential distribution of channel types.

Distribution of presynaptic varicosities in Neurobiotin-filled axons

A simple explanation for the axonal spots with larger $\Delta F/F_o$ responses would be that they correspond to presynaptic *en passant* boutons, where clusters of voltage-dependent Ca^{2+} channels are activated after AP stimulation. We searched for a confirmation of this hypothesis by comparing the spatial density of hot spots measured in fluorescence imaging experiments with morphological information on inter-bouton spacing obtained from analysis of the axons of Neurobiotin-

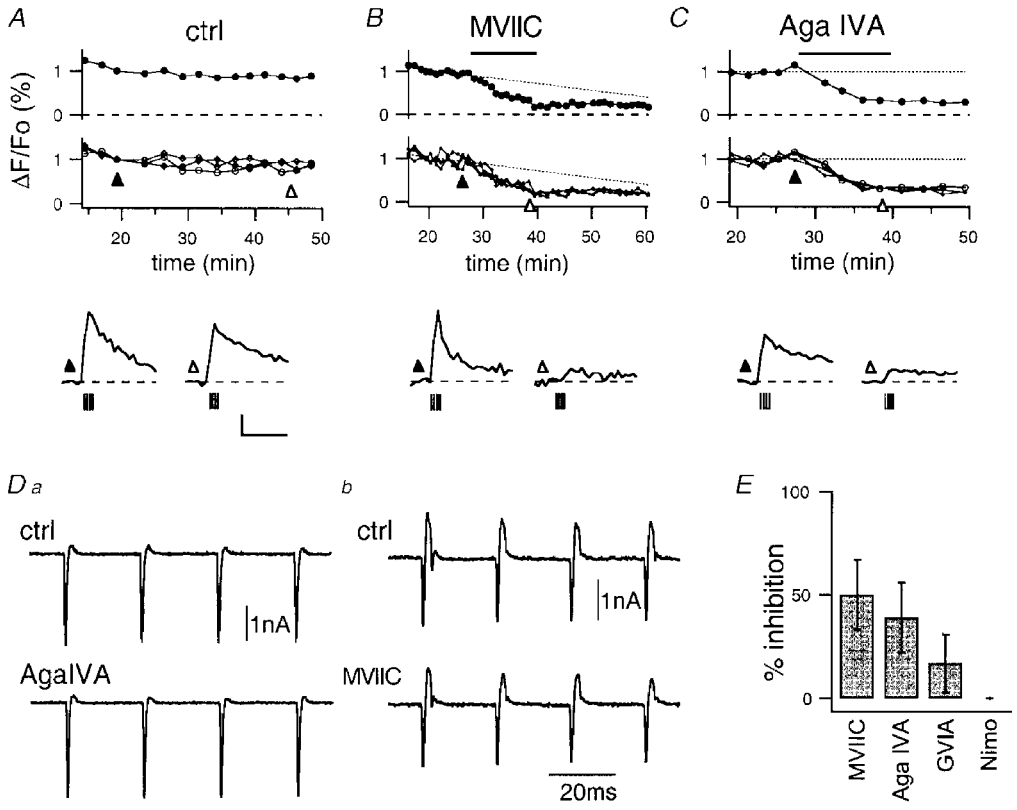

Figure 6. Effects of Ca^{2+} channel blockers on axonal hot spot Ca^{2+} signals

Effects of bath application of Ca^{2+} channel blockers on peak $\Delta F/F_o$ hot spot responses (*A–C*; > 100 μm from soma) and on somatic voltage-gated currents (*D*) upon stimulation of basket (*B*) and stellate (*A* and *C*) interneurones with a train of 4 APs, 43 Hz. *A–C*, plots of peak $\Delta F/F_o$ response *vs.* WCR time from individual axonal hot spots (middle graphs), or averaged across hot spots (top graphs), in 3 different axons. Period of drug application in *B* and *C* is indicated by bars. Bottom traces: representative $\Delta F/F_o$ traces for a selected hot spot from each axon, during AP stimulation (indicated by vertical bars) at WCR times indicated by triangles in corresponding middle panels. Scale bars: 600 ms, 50 % (*A*); 600 ms, 42 % (*B* and *C*). *A*, control experiment, no drug application. *B* and *C*, application of 5 μM ω-CgTX-MVIIC (*B*), 500 nM ω-Aga-IVA (*C*). *D*, representative traces of somatic whole-cell recorded currents during AP train stimulation from two experiments using perfusion of ω-Aga-IVA (*Da*), or ω-CgTX-MVIIC (*Db*; same experiment as panel *B*), performed with a 2-photon excitation laser scanning apparatus. Top and bottom traces are taken during control conditions and after drug perfusion, respectively. *E*, summary plot of Ca^{2+} channel blockers (ω-CgTX-MVIIC, ω-Aga-IVA, ω-conotoxin GVIA, nimodipine) effects on peak $\Delta F/F_o$. Columns represent inhibition (mean ± S.D.) of averaged hot spot peak $\Delta F/F_o$. Number of experiments averaged in each column are 4 (MVIIC), 6 (Aga IVA), 4 (GVIA) and 5 (Nimo).

filled interneurones. The morphology of 10 Neurobiotin-filled interneurones from young rats (12–15 days old) was studied and the density of *en passant* varicosities was obtained. Five interneurones were basket cells, as defined by the presence of a basket structure (Ramón y Cajal, 1911) on the somata of Purkinje cells ($n = 1$), or, in the absence of a clear basket structure, by the position of the cell body in the lower third of the molecular layer and the presence of a main axon branch running parallel to the Purkinje cell layer and sending numerous collaterals at right angles in the direction of Purkinje cell bodies ($n = 4$). Another five interneurones had somata in the middle or upper third of the molecular layer, and conformed to the descriptions of a 'deep' or 'superficial' stellate cell given by Ramón y Cajal (1911).

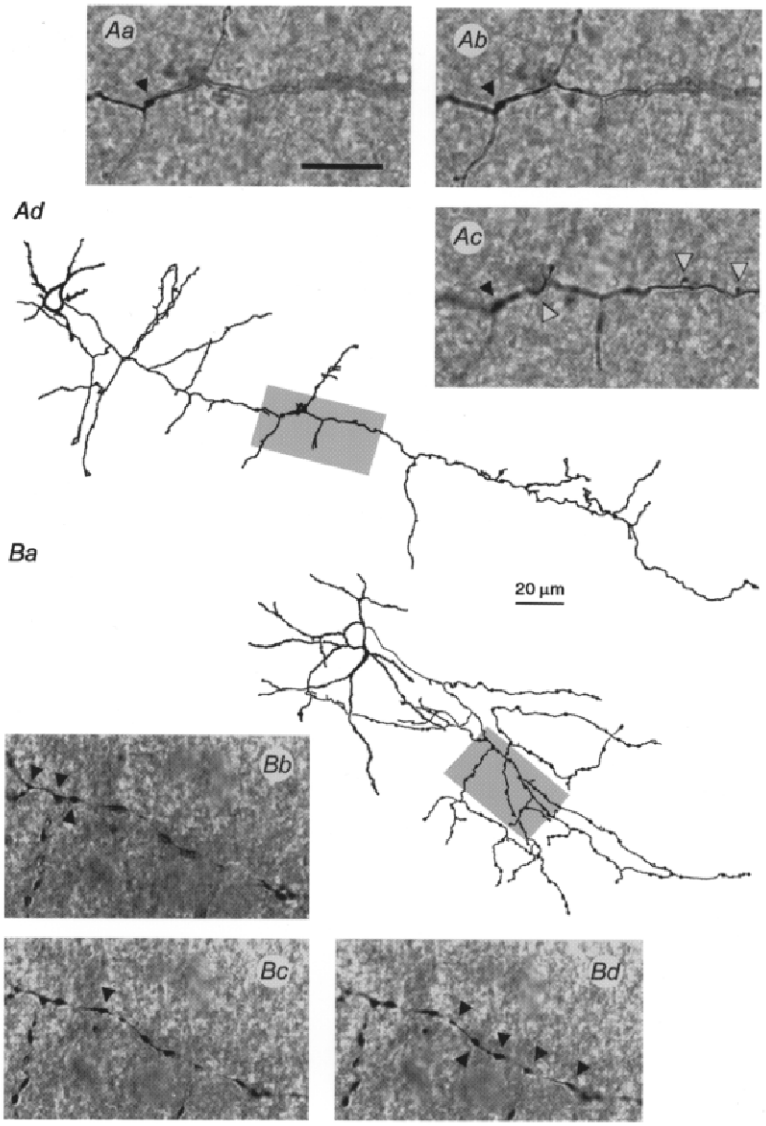

Figure 7. Axonal varicosities in Neurobiotin-filled axons of P12–P16 interneurones

Analysis of the axon morphology of two Neurobiotin-filled P14 stellate cells. The interneurone in *A* (middle portion of the molecular layer, VIth lobule) is representative of 80 % of the cells examined, while the cell in *B* (middle portion of the molecular layer, IVth lobule) is one of two with 'adult-like' axonal morphology found at this age. *Aa*, *b* and *c*, photographs of a portion of the main axon branch (indicated by shaded area in *Ad*) taken in three different focal planes displaced by 2·3 µm (*Aa* to *Ab*) and 2·5 µm (*Ab* to *Ac*). A single varicosity (large ovoid structure) is present in this area, visible in each image (black arrowheads). Very short emerging branches are visible in *Ac* (white arrowheads). The entire axonal ramification was 1102 µm long and presented 12 varicosities. Calibration bar in *Aa* (10 µm) also applies to *Ab* and *c*, *Bb*, *c* and *d*. Drawings of cells (*Ad* and *Ba*) show the axon as a thin line and the soma and dendrites as thick lines. Varicosities identified on the axon are rendered with a black dot (not to scale with the original drawing). *Bb*, *c* and *d*, photographs of a portion of the main axon branch (shaded area in *Ba*) at focal planes lying 0·8 µm (*Bb* to *c*) and 0·9 µm (*Bc* to *d*) apart. Notice the frequent varicosities (indicated, for the main axon only, by arrowheads). The length of the entire axonal ramification was 1608 µm; there were 116 varicosities, on average 13·9 µm apart.

Axonal varicosities were defined as ovoid structures, with a diameter severalfold larger than the diameter of the incoming axon, visible in different focal planes when focusing across the axon up and down by a few micrometres, as exemplified in Fig. 7. In five basket and three stellate cells, the axons tended to present an irregular diameter and frequent thickenings or short collateral branches a few micrometres long, but clearly defined varicosities were rare (Fig. 7*A*). Mean distances between varicosities ranged from 21 to 92 μm (average: 45 ± 24 μm), with 11–29 boutons per axonal tree, and 230–1540 μm overall axonal lengths (all distances and lengths reported here are a lower estimate, as explained in Methods). In the remaining two stellate cells (Fig. 7*B*), varicosities were more abundant (42 and 116, with axonal trees of 190 and 1610 μm length, i.e. with mean distances of 4·5 and 13·9 μm, respectively), closer to the situation for 21- to 34-day-old rats, where the average distance between varicosities was reported to be $6{\cdot}8 \pm 2$ μm (analysis from four axons of stellate cells from Pouzat & Kondo, 1996). These results show that presynaptic specialisations had not developed to a mature morphology in the P12–P15 rats used in this study.

From the above results, it is clear that the density of hot spots in imaging experiments was larger than that of morphologically identified axonal varicosities. However, as the former is comparable with the spacing of varicosities in axons from more mature (⩾P21) animals, the hypothesis that hot spots represent Ca^{2+} sources localised at the site of developing presynaptic *en passant* boutons remains open, as will be discussed more extensively later. Our attempts to study fluorescence responses in axons from mature animals did not succeed, because, in our hands, the chance of surviving the slicing procedure was low for mature interneurones, and moreover the diffusion of dye into the axon was insufficient for imaging, possibly due to the smaller diameter of mature axons (Larramendi, 1969). As a consequence, we could not check for the correlation of distributions of hot spots and boutons in adults. In three interneurones from younger animals (postnatal day 7), the axonal $[Ca^{2+}]$ responses were analysed along 12, 34 and 60 μm long regions during responses to 8 AP stimuli. There were no hot spots (1 cell), or only small-amplitude hot spots (1 spot in 60 μm in one case, and 4 in 34 μm in the last case), with peak $\Delta F/F_o$ in the range 50–60 %, corresponding to ~1/3 of the average response to 8 APs in P12–P16 animals. The remaining axonal areas displayed slower and smaller (~10–20 % at peak) responses, indicating a low, nearly homogeneous density of Ca^{2+} sources.

$[Ca^{2+}]$ signals at axonal bifurcations

In Cs^+-loaded cerebellar basket cells, points of axonal bifurcation were found to respond to depolarisation with $[Ca^{2+}]$ rises of comparable magnitude to those elicited by the

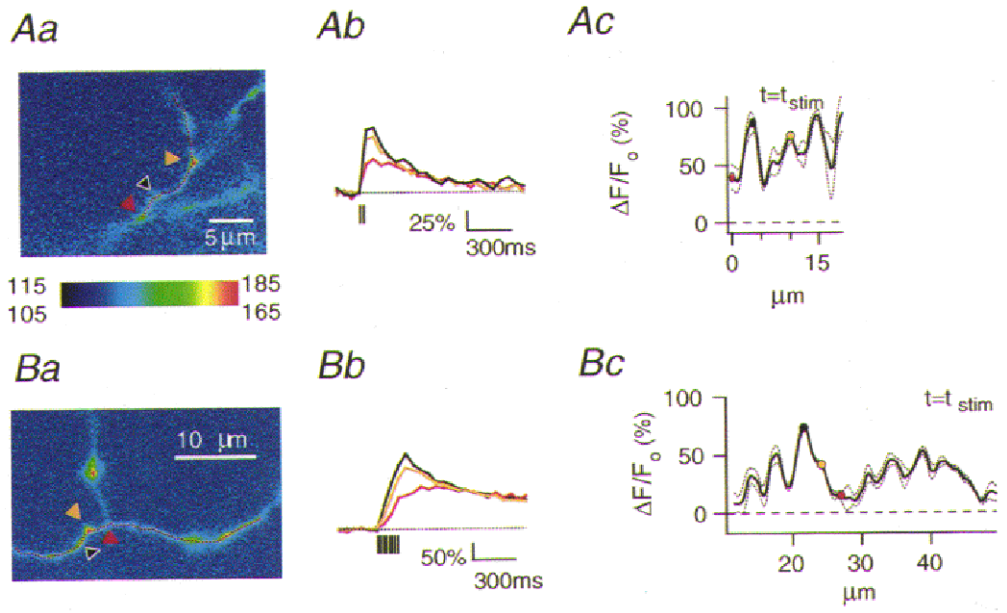

Figure 8. Calcium signals at axonal branch points

A and *B*, examples of $\Delta F/F_o$ behaviour at two branching points. *Aa* and *Ba*, images of consecutive bifurcations of a 1st order collateral branch for a P14 interneurone (*Aa*; ~150–160 μm from the soma; 2 AP stimulation), and of a bifurcation of the main axon branch for a P13 interneurone (*Ba*; ~110 μm from soma; 8 AP stimulation). Third image after stimulus onset. *Ab* and *Bb*, time course of $\Delta F/F_o$ in three different axonal sites. These sites are identified in the images in *Aa* and *Ba* by arrowheads of colour corresponding to trace colour. In *A*, the branch point marked in yellow behaved as a hot spot, whereas in *B*, the bifurcation point (marked by the red arrow) had a longer rise time and smaller peak amplitude with respect to the sites identified in black and yellow. *Ac* and *Bc*, plot of $\Delta F/F_o^{stim}$ (thick line) and $\Delta F/F_o^{stim} \pm \sigma$ (dotted lines) *vs.* position in the axon. Black, red and yellow circles indicate $\Delta F/F_o^{stim}$ for positions marked with arrowheads of corresponding colours in *Aa* and *Ba*.

same stimuli at axonal varicosities and terminals (Llano *et al.* 1997). We therefore looked at the action potential-evoked $[Ca^{2+}]$ rises using the more stringent criteria for hot spot detection introduced above. $\Delta F/F_o$ at axonal branch points had variable properties. Eight out of 20 analysed bifurcations (13 cells) behaved as hot spots, as the site marked in yellow in Fig. 8*A* (see also Fig. 3*B*, spot at $i = 27$ μm). In seven other cases, the branch point lay close to a minimum for $\Delta F/F_o^{stim}$, in an area with lower and slower $[Ca^{2+}]$ responses than those of hot spots (Fig. 8*B*). The remaining bifurcations, that could not be defined as hot spots (either because of noise limitations, or because they did not correspond to a local maximum for $\Delta F/F_o^{stim}$), had $\Delta F/F_o$ with fast rise time but smaller peak amplitude with respect to hot sites nearby in the axon (see site marked in red in Fig. 8*A*). The hot and cold response type was found in two cases at consecutive branch points of a single axon.

Under the hypothesis that hot spots in axons are randomly distributed, we can estimate the expected fraction of bifurcations coinciding by chance with a hot spot using the measured inter-hot spot distance distribution. Assuming an uncertainty of ± 2 pixels (pixel size: 0·25 μm) in the choice of the exact location of the branch point, and using our measured value of mean hot spot density ($0{\cdot}21 \pm 0{\cdot}07$ μm^{-1}), the expected fraction would be $0{\cdot}26 \pm 0{\cdot}08$. Over an ensemble of 15 bifurcations that could be clearly identified either as a hot or a cold spot, the fraction of hot spots was 8/15, i.e. 0·53. This is higher than expected from a chance occurrence of Ca^{2+} sources in branching points, corresponding to about 4 ± 1 bifurcations. The coincidence of hot spots with bifurcations could have important functional consequences, which deserve further investigation.

DISCUSSION

Our study resolves for the first time $[Ca^{2+}]$ signals evoked by action potentials along continuous stretches of unmyelinated CNS axons, avoiding the arbitrary selection of regions of interest. We show a non-artefactual heterogeneous spatial pattern for the axonal $[Ca^{2+}]$ transients evoked by AP stimulation in young rats, with sequences of hot spots spaced by ~5 μm, defined as sites on the axon where the peak $\Delta F/F_o$ response had a local maximum. We show that pharmacological block of specific voltage-dependent Ca^{2+} channel types decreases Ca^{2+} rises in hot spots, with a prominent role of P/Q-type channels. We further show that, in the P12–P16 rats used for the present study, morphologically mature presynaptic varicosities are rare, ~10 times less abundant than sites presenting large Ca^{2+} responses. We discuss below a hypothesis on the morphological and functional identity of these strongly responsive axonal sites.

Ca^{2+} channel types involved in hot spot Ca^{2+} rises

$[Ca^{2+}]$ transients evoked by a short AP train in hot spots of cerebellar interneurones were largely decreased by the toxin ω-CgTX-MVIIC, at a dose which is nearly saturating for inhibition of N- and P/Q-type channels (Hillyard *et al.* 1992; Randall & Tsien, 1995; McDonough *et al.* 1996). The slow time course of inhibition and the absence of visible recovery upon toxin wash-out would suggest a negligible contribution from N-type channels, for which block by ω-CgTX-MVIIC is fast, potent and reversible (Grantham *et al.* 1994; McDonough *et al.* 1996), even with physiological bath solutions (McDonough *et al.* 1996). In addition, the specific N-type channel blocker ω-conotoxin GVIA had little to no effect, strengthening the hypothesis that N-type channels have little role in generating the axonal Ca^{2+} signals. On the contrary, the P/Q-type blocker ω-Aga-IVA (Mintz *et al.* 1992; Randall & Tsien, 1995) had a large inhibitory effect, indicating that most of the ω-CgTX-MVIIC effect was exerted on P/Q-type channels. Interestingly, in a recent comprehensive study of postnatal changes in Ca^{2+} channels mediating central synaptic transmission (Iwasaki *et al.* 2000), it has been shown that P-type channels tend to be developmentally upregulated at the expense of N-type channels in presynaptic terminals of various (but not all) brain regions, including, in the cerebellum, at the synapses formed by Purkinje cells onto deep cerebellar nuclei neurones. The small excess inhibition found in our experiments by ω-CgTX-MVIIC with respect to ω-Aga-IVA, although not significant, might indicate a contribution from block of N-type channels, as well as from some R-type channels. In fact, ω-CgTX-MVIIC block of Ca^{2+} currents insensitive to ω-conotoxin GVIA and to high concentrations of ω-Aga-IVA (1 μM) has been reported in some preparations (Wu & Saggau, 1995; McDonough *et al.* 1996). Application of ω-CgTX-MVIIC in our study left unaffected ~50% of the axonal Ca^{2+} signals. This could result from imperfect control of drug concentration in the slice and/or from the reported slowing of toxin binding to P-type channels by bath cations, and especially by Ca^{2+} (McDonough *et al.* 1996). Alternatively, the unblocked signal could arise from the presence of some additional unidentified mechanisms allowing AP-evoked Ca^{2+} influx in the axon. Possible candidates are ω-CgTX-MVIIC-insensitive R-type Ca^{2+} channels, which have been found to mediate, in axons, a small fraction of Ca^{2+} influx in the MNTB of young rats (Wu *et al.* 1998), and to be responsible for oxytocin secretion in the adult rat neurohypophysis (Wang *et al.* 1999).

In the adult cerebellar cortex, mRNA transcripts for the Ca^{2+} channel subunits α_{1B}, α_{1A} and α_{1E}, which form the pore region of N-, P/Q- and R-type channels, respectively (discussed by Dunlap *et al.* 1995; Beam, 1999; Tottene *et al.* 2000), have been revealed by *in situ* hybridization (in rats: Ludwig *et al.* 1997, and references therein; in humans: Volsen *et al.* 1995). In the molecular layer, immuno-cytochemical studies have detected the presence of α_{1B} and α_{1A} in Purkinje cell (PC) dendrites and in presumed impinging presynaptic terminals (Westenbroek *et al.* 1992, 1995). In particular, α_{1A} immunoreactivity seemed to be present both on spine- and shaft-contacting presynaptic structures (Westenbroek *et al.* 1995), as well as in basket cell somata (Volsen *et al.* 1995). Anti-α_{1E} antibodies stained

weakly and diffusely the molecular layer (Volsen *et al.* 1995), and were visible on fine dendrites and branching points of Purkinje cells (Yokohama *et al.* 1995). At the inhibitory interneurone to Purkinje cell connection, Ca^{2+} channel types controlling evoked transmission have been studied by Doroshenko *et al.* (1997) by monitoring the frequency and amplitude of spontaneous IPSCs (sIPSCs) in young rats, and no effects of ω-CgTX-MVIIC, ω-Aga-IVA or ω-conotoxin GVIA were detected. We observed a clear, large effect of the first two toxins on axonal AP-evoked Ca^{2+} signals of stellate and basket interneurones. The toxin effects were homogeneous in axons, and it would be difficult to imagine that no presynaptic terminals were present in the imaged areas. The effect of toxins could have been undetected in the study of Doroshenko *et al.* (1997) if the recorded sIPSCs contained a large percentage of mIPSCs, as these events would reflect spontaneous GABA release which is independent of AP and subsequent Ca^{2+} influx.

The effects of Ca^{2+} channel blockers on axonal Ca^{2+} responses in our recordings could be produced by a direct block of channels resident in the axon, as well as from block of distant channels controlling the generation and/or shape of AP trains. The latter mechanism is, however, less likely to be involved. As described above, we did not see changes in somatic inward (Na^+) currents during AP train stimulation. Likewise, no effect of ω-CgTX-MVIIC on the shape of somatic AP trains was reported by Christie *et al.* (1995) in rat hippocampal CA1 pyramidal neurones. During low frequency stimulation, the shape and amplitude of the extracellularly recorded presynaptic volley were unaltered by ω-CgTX-MVIIC, ω-Aga-IVA or ω-conotoxin GVIA in area CA1 of guinea-pig hippocampus (Wu & Saggau, 1995) and in the molecular layer of rat cerebellum (Mintz *et al.* 1995). Furthermore, in the neonatal rat optic nerve, application of the same toxins did not affect propagation and waveform of short AP trains, while the presence of axonal N-type channels producing large Ca^{2+} rises was revealed (Sun & Chiu, 1999). In summary, the available information suggests that calcium channel block should not affect waveform and propagation of short AP trains as used in our study, and that inhibition of axonal Ca^{2+} signals is best explained by block of local Ca^{2+} channel activation in the axon.

The spatial heterogeneity of axonal $[Ca^{2+}]$ responses: relationship of hot spots with developing synapses?

A parsimonious explanation for the nature of hot spots would be that they are related to presynaptic release sites, where clusters of voltage-dependent Ca^{2+} channels are activated upon AP propagation (with possible additional contributions from clustering of other types of molecules related to Ca^{2+} mobilisation, namely intracellular-release Ca^{2+} channels, and Ca^{2+} buffering, sequestration and extrusion systems). The following arguments support this view. Unmyelinated adult axons in several cortical areas present a sequence of varicosities distributed at intervals of a few micrometres (Braitenberg & Schüz, 1991). In the neocortex, varicosities were shown to be presynaptic terminals with virtually a 1:1 relationship (as determined by the presence, in electronmicrographs, of clusters of small synaptic vesicles and presynaptic specialisations; Hellwig *et al.* 1994, and references therein). Axonal varicosities have been observed in ultrastructural studies of the molecular layer of adult rat cerebellum (Palay & Chan-Palay, 1974). Two light-microscopy studies reported quantitative estimates of the mean density of varicosities on axons of Neurobiotin-filled rat interneurones, which were 0·15 boutons μm^{-1} for young adults (21–34 days old; Pouzat & Kondo, 1996), and 0·11 boutons μm^{-1} in 3-month-old animals (with a lower density for deep than for superficial interneurones; Sultan & Bower, 1998). In basket and stellate cells from P12–P16 rats, we find a very low mean density of clearly detectable boutons ($< 0{\cdot}022\ \mu m^{-1}$), around tenfold lower than the density of hot spots ($0{\cdot}21\ \mu m^{-1}$). However, the latter value is comparable to the above mentioned density of axonal varicosities in mature animals. Therefore, we hypothesise that hot spots represent sites of high Ca^{2+} influx localised at the position of developing presynaptic *en passant* boutons. A further observation in accordance with this hypothesis is that sIPSCs in interneurones and Purkinje cells are rarely detected at P7 (authors' unpublished observations), while in the age range P12–P16 they are much more frequent (Vincent *et al.* 1992), suggesting that fewer synaptic contacts exist at P7, an age when interneurones only begin to appear in the molecular layer (Altman, 1971). Correspondingly, imaging experiments performed with AP stimulation in P7 axons revealed a very low hot spot density.

The proposal of VDCCs accumulation at developing presynaptic sites before formation of a mature bouton is supported by a few considerations. Ultrastructural studies on large, mature terminals have shown clusters of particles suggested to be voltage-dependent Ca^{2+} channels (e.g. Pumplin *et al.* 1981). An ultrastructural description of phases of synaptic development in the cerebellum was given by Larramendi (1969) in the case of parallel fibre *en passant* boutons, showing that formation of pre- and postsynaptic densities precedes accumulation of synaptic vesicles and mitochondria and appearance of varicosities. From the molecular point of view, no reports are available, to our knowledge, on the developmental changes of density and types of axonal VDCCs. However, changes in presynaptic Ca^{2+} channel types controlling AP-evoked transmitter release have been reported in various systems (Verderio *et al.* 1995; Iwasaki *et al.* 2000, and references therein).

Extrasynaptic $[Ca^{2+}]$ signals

The origin of $[Ca^{2+}]$ responses in regions outside hot spots in P12–P16 axons remains unclear. Our pharmacological studies did not support the notion that different Ca^{2+} channel types exist in terminals *vs.* axon. The small signals in cold regions could be explained by diffusion from nearby hot spots, as well as by a lower density of extrasynaptic Ca^{2+} sources. Further improvement in the spatial and temporal resolution of imaging experiments will be needed to clarify this point.

On the other hand, diffusion cannot account for the small, sparse [Ca^{2+}] responses (noticeably in a 60 μm long axon that bore only one hot spot) observed in P7 axons, which suggest a low, homogeneous Ca^{2+} source density.

Reliability of AP propagation in imaging experiments

Failures of AP propagation in axons have been observed in several vertebrate and invertebrate preparations, either at high stimulation frequencies or, in some cases, at lower frequencies (reviewed in Wall, 1995). In the age window considered in our study, failures of AP propagation are among the mechanisms proposed to explain the large variability of IPSCs observed in paired interneurone–Purkinje cell recordings with low-frequency stimulation (Vincent & Marty, 1996). In those recordings, data were acquired during the first few minutes after the start of presynaptic dialysis. Here, we recorded AP-evoked [Ca^{2+}] signals ($\leqslant$ 0·5 Hz) at later times ($>$8 min) after the start of WCR. In spite of considerable run-down of Na^+ currents during this period, APs were always safely generated and propagated up to $>$150 μm from the cell soma past several branching points in the main branch, as well as at $>$100 μm distance in first and second order collateral branches. Thus, in accordance with previous fluorescence imaging studies (Mackenzie *et al.* 1996; Frenguelli & Malinow, 1996), in our conditions failures are absent, and axonal bifurcations do not behave as points of conduction block, as observed elsewhere (reviewed in Wall, 1995) and predicted from theoretical studies (reviewed in Swadlow *et al.* 1980). However we stress that our measurements are made after extensive dialysis of the cytosol, and that the possibility of propagation failures at earlier WCR times cannot be ruled out.

Altman, J. (1972). Postnatal development of the cerebellar cortex in the rat. The external germinal layer and the transitional molecular layer. *Journal of Comparative Neurology* **145**, 353–398.

Bacskai, B. J., Wallén, P., Lev-Ram, V., Grillner, S. & Tsien, R. Y. (1995). Activity-related calcium dynamics in lamprey motoneurons as revealed by video-rate confocal microscopy. *Neuron* **14**, 19–28.

Beam, K. (1999). Calcium channel splicing: mind your Ps and Qs. *Nature Neuroscience* **2**, 393–414.

Borst, J. G. G., Helmchen, F. & Sakmann, B. (1995). Pre- and postsynaptic whole-cell recordings in the medial nucleus of the trapezoid body of the rat. *Journal of Physiology* **489**, 825–840.

Braitenberg, V. & Schüz, A. (1991). *Anatomy of the Cortex.* Springer-Verlag, Berlin.

Callewaert, G., Eilers, J. & Konnerth, A. (1996). Axonal calcium entry during fast 'sodium' action potentials in rat cerebellar Purkinje neurones. *Journal of Physiology* **495**, 641–647.

Christie, B. R., Eliot., L. S., Ito, K.-I., Miyakawa, H. & Johnston, D. (1995). Different Ca^{2+} channels in soma and dendrites of hippocampal neurons mediate spike-induced Ca^{2+} influx. *Journal of Neurophysiology* **73**, 2553–2557.

David, G., Barrett, J. N. & Barrett, E. F. (1997). Stimulation-induced changes in [Ca^{2+}] in lizard motor nerve terminals. *Journal of Physiology* **504**, 83–96.

Delaney, K., Tank, D. W. & Zucker, R. S. (1991). Presynaptic calcium and serotonin-mediated enhancement of transmitter release at crayfish neuromuscular junction. *Journal of Neuroscience* **11**, 2631–2643.

Doroshenko, P. A., Woppmann, A., Miljanich, G. & Augustine, G. J. (1997). Pharmacologically distinct presynaptic calcium channels in cerebellar excitatory and inhibitory synapses. *Neuropharmacology* **36**, 865–872.

Dunlap, K., Luebke, J. I. & Turner, T. J. (1995). Exocytotic Ca^{2+} channels in mammalian central neurons. *Trends in Neurosciences* **18**, 89–98.

Frenguelli, B. G. & Malinow, R. (1996). Fluctuations in intracellular calcium responses to action potentials in single *en passage* presynaptic boutons of layer V neurons in neocortical slices. *Learning and Memory* **3**, 150–159.

Grantham, C. J., Bowman, D., Bath, C. P., Bell, D. C., Bleakman, D. (1994). ω-Conotoxin MVIIC reversibly inhibits a human N-type calcium channel and calcium influx into chick synaptosomes. *Neuropharmacology* **33**, 255–258.

Hellwig, B., Schüz, A. & Aertsen., A. (1994). Synapses on axon collaterals of pyramidal cells are spaced at random intervals: a Golgi study in the mouse cerebral cortex. *Biological Cybernetics* **71**, 1–12.

Helmchen, F., Borst, J. G. G. & Sakmann, B. (1997). Calcium dynamics associated with a single action potential in a CNS presynaptic terminal. *Biophysical Journal* **72**, 1458–1471.

Hillyard, D. R., Monje, V. D., Mintz, I. M., Bean, B. P., Nadasdi, L., Ramachandran, J., Miljianich, G., Azimi-Zoonooz, A., McIntosh, J. M., Cruz, L. J., Imperial, J. S. & Olivera, B. M. (1992). A new Conus peptide ligand for mammalian presynaptic Ca^{2+} channels. *Neuron* **9**, 69–77.

Iwasaki, S., Momiyama, A., Uchitel, O. D. & Takahashi, T. (2000). Developmental changes in calcium channel types mediating central synaptic transmission. *Journal of Neuroscience* **20**, 59–65.

Kriegstein, A. R. & Dichter, M. A. (1983). Morphological classification of rat cortical neurons in cell culture. *Journal of Neuroscience* **3**, 1634–1647.

Larramendi, L. M. H. (1969). Analysis of synaptogenesis in the cerebellum of the mouse. In *Neurobiology of Cerebellar Evolution and Development*, ed. Llinás, R., pp. 803–843. American Medical Association, Chicago.

Llano, I., Tan, Y. P. & Caputo, C. (1997). Spatial heterogeneity of intracellular Ca^{2+} signals in axons of basket cells from rat cerebellar slices. *Journal of Physiology* **502**, 509–519.

Llinás, R., Sugimori, M. & Silver, R. B. (1992). Microdomains of high calcium concentration in a presynaptic terminal. *Science* **256**, 677–679.

Ludwig, A., Flockerzi, V. & Hofmann, F. (1997). Regional expression and cellular localization of the α_1 and β subunit of high voltage-activated calcium channels in rat brain. *Journal of Neuroscience* **17**, 1339–1349.

Lüscher, C., Lipp, P., Lüscher, H.-R. & Niggli, E. (1996). Control of action potential propagation by intracellular Ca^{2+} in cultured rat dorsal root ganglion cells. *Journal of Physiology* **490**, 319–324.

McDonough, S. I., Swartz, K. J., Mintz, I. M., Boland, L. M. & Bean, B. P. (1996). Inhibition of calcium channels in rat central and peripheral neurons by ω-conotoxin MVIIC. *Journal of Neuroscience* **16**, 2612–2623.

Mackenzie, P. J., Umemiya, M. & Murphy, T. H. (1996). Ca^{2+} imaging of CNS axons in culture indicates reliable coupling between single action potentials and distal functional release sites. *Neuron* **16**, 783–795.

Mintz, I. M., Adams, M. E. & Bean, B. P. (1992). P-type calcium channels in central and peripheral neurons. *Neuron* **9**, 1–20.

Mintz, I. M., Sabatini, B. L. & Regehr, W. G. (1995). Calcium control of transmitter release at a cerebellar synapse. *Neuron* **15**, 675–688.

Ogden, D. (1996). Intracellular calcium release in central neurons. *Seminars in the Neurosciences* **8**, 281–291.

Palay, S. L. & Chan-Palay, V. (1974). *Cerebellar Cortex, Cytology and Organization*, chaps VII–VIII. Springer, Berlin.

Pouzat, C. & Hestrin, S. (1997). Developmental regulation of basket/stellate →Purkinje cell synapses in the cerebellum. *Journal of Neuroscience* **17**, 9104–9112.

Pouzat, C. & Kondo, S. (1996). An analysis of neurobiotin-filled stellate axons in the rat cerebellum. *Society for Neuroscience Abstracts* **22**, 1632.

Pouzat, C. & Marty, A. (1999). Somatic recording of GABAergic autoreceptor current in cerebellar stellate and basket cells. *Journal of Neuroscience* **19**, 1675–1690.

Pumplin, E. F., Reese, E. F. & Llinás, R. (1981). Are the presynaptic membrane particles the calcium channels? *Proceedings of the National Academy of Sciences of the USA* **78**, 7210–7213.

Ramón y Cajal, S. (1911). *Histologie du système nerveux de l'homme et des vertebrés*. Maloine, Paris.

Randall, A. & Tsien, R. W. (1995). Pharmacological dissection of multiple types of Ca^{2+} channel currents in rat cerebellar granule neurons. *Journal of Neuroscience* **15**, 2995–3012.

Schiller, J., Helmchen, F. & Sakmann, B. (1995). Spatial profile of dendritic calcium transients evoked by action potentials in rat neocortical pyramidal neurons. *Journal of Physiology* **487**, 583–600.

Sultan, F. & Bower, J. M. (1998). Quantitative Golgi study of the rat cerebellar molecular layer interneurons using principal component analysis. *Journal of Comparative Neurology* **393**, 353–373.

Sun, B. B. & Chiu, S. Y. (1999). N-type calcium channels and their regulation by $GABA_B$ receptors in axons of neonatal rat optic nerve. *Journal of Neuroscience* **19**, 5185–5194.

Swadlow, H. A., Kocsis, J. D. & Waxman, S. G. (1980). Modulation of impulse conduction along the axonal tree. *Annual Review of Biophysics and Bioengineering* **9**, 143–179.

Tan, Y. P. & Llano, I. (1999). Modulation by K^+ channels of action potential-evoked intracellular Ca^{2+} concentration rises in rat cerebellar basket cell axons. *Journal of Physiology* **520**, 65–78.

Tottene, A., Volsen, S. & Pietrobon, D. (2000). α_{1E} subunits form the pore of three cerebellar R-type calcium channels with different pharmacological and permeation properties. *Journal of Neuroscience* **20**, 171–178.

Verderio, C., Coco, S., Fumagalli, G. & Matteoli, M. (1995). Calcium-dependent glutamate release during neuronal development and synaptogenesis: different involvment of ω-agatoxin IVA- and ω-conotoxin GVIA-sensitive channels. *Proceedings of the National Academy of Sciences of the USA* **92**, 6449–6453.

Vincent, P., Armstrong, C. M. & Marty, A. (1992). Inhibitory synaptic currents in rat cerebellar Purkinje cells: modulation by postsynaptic depolarization. *Journal of Physiology* **456**, 453–471.

Vincent, P. & Marty, A. (1996). Fluctuations of inhibitory postsynaptic currents in Purkinje cells from rat cerebellar slices. *Journal of Physiology* **494**, 183–199.

Volsen, S. G., Day, N. C., McCormack, A. L., Smith, W., Craig, P. J., Beattie, R., Ince, P. G., Shaw, P. J., Ellis, S. B., Gillespie, A., Harpold, M. M. & Lodge, D. (1995). The expression of neuronal voltage-dependent calcium channels in human cerebellum. *Molecular Brain Research* **34**, 271–282.

Wächtler, J., Mayer, C. & Grafe, P. (1998). Activity-dependent intracellular Ca^{2+} transients in unmyelinated nerve fibers of the isolated rat vagus nerve. *Pflügers Archiv* **435**, 678–686.

Wall, P. D. (1995). Do nerve impulses penetrate terminal arborizations? A pre-presynaptic control mechanism. *Trends in Neurosciences* **18**, 99–103.

Wang, G., Dayanithi, G., Newcomb, R. & Lemos, J. R. (1999). An R-type Ca^{2+} current in neurohypophysial terminals preferentially regulates oxytocin secretion. *Journal of Neuroscience* **19**, 9235–9241.

Westenbroek, R. E., Hell, J. W., Warner, C., Dubel, S. J., Snutch, T. P. & Catterall, W. A. (1992). Biochemical properties and subcellular distribution of an N-type Ca^{2+} channel α_1 subunit. *Neuron* **9**, 1099–1115.

Westenbroek, R. W., Sakurai, T., Elliott, E. M., Hell, J. W., Starr, T. V., Snutch, T. P. & Catterall, W. A. (1995). Immunochemical identification and subcellular distribution of the α_{1A} subunits of brain Ca^{2+} channels. *Journal of Neuroscience* **15**, 6403–6418.

Wu, L.-G., Borst, J. G. G. & Sakmann, B. (1998). R-type Ca^{2+} currents evoke transmitter release at a rat central synapse. *Proceedings of the National Academy of Sciences of the USA* **95**, 4720–4725.

Wu, L.-G. & Saggau, P. (1995). Block of multiple presynaptic calcium channel types by ω-conotoxin-MVIIC at hippocampal CA3 to CA1 synapses. *Journal of Neurophysiology* **23**, 1965–1972.

Wu, L.-G., Westenbroek, R. E., Borst, J. G. G., Catterall, W. A. & Sakmann, B. (1999). Calcium channel types with distinct presynaptic localization couple differentially to transmitter release in single calyx-type synapses. *Journal of Neuroscience* **19**, 726–736.

Yokohama, C. T., Westenbroek, R. E., Hell, J. W., Soong, T. W., Snutch, T. P. & Catterall, W. A. (1995). Biochemical properties and subcellular distribution of the neuronal class E calcium channel α_1 subunit. *Journal of Neuroscience* **15**, 6419–6432.

Acknowledgements

We thank Arturo Hernandez-Cruz, Alain Marty and Roberta Rivosecchi for critical comments on the manuscript, Yusuf Tan for help with analysis routines and Angelita Tottene for testing our nimodipine stock. This work was supported by the Max-Planck Gesellschaft. L.F. was the recipient of a Marie Curie Research Training Grant from the European Community (no. ERBFMBICT 971952).

Corresponding author

L. Forti: Dipartimento di Fisiologia e Farmacologia cellulari e molecolari, Sezione di Fisiologia Generale, Universita' di Pavia, Via Forlanini 6, 27100 Pavia, Italy

Email: lforti@unipv.it

Authors' present addresses

L. Forti: Dipartimento di Fisiologia Generale, Universita' di Pavia, Via Forlanini 6, 27100 Pavia, Italy.

C. Pouzat: Caltech, Biology Division, 139–174, Pasadena, CA 91125, USA.